ACS APPLIED MATERIALS & INTERFACES

RESEARCH ARTICLE

www.acsami.org

Freestanding Ultrananocrystalline Diamond Films with Homojunction Insulating Layer on Conducting Layer and Their High Electron Field Emission Properties

Joseph P. Thomas,[†,*,‡] Huang-Chin Chen,[†] Nyan-Hwa Tai,[‡] and I-Nan Lin[*,†]

[†]Department of Physics, Tamkang University, Tamsui 251, Taiwan, R.O.C.

[‡]Department of Materials Science and Engineering, National Tsing-Hua University, Hsinchu 300, Taiwan, R.O.C.

ABSTRACT: Freestanding ultrananocrystalline diamond (UNCD) films with homojunction insulating layer in situ grown on a conducting layer showed superior electron field emission (EFE) properties. The insulating layer of the films contains large dendrite type grains (400−600 nm in size), whereas the conducting layer contains nanosize equi-axed grains (5−20 nm in size) separated by grain boundaries of about 0.5−1 nm in width. The conducting layer possesses n-type (or semimetallic) conductivity of about 5.6×10^{-3} $(\Omega\ \mathrm{cm})^{-1}$, with sheet carrier concentration of about 1.4×10^{12} cm^{-2}, which is ascribed to in situ doping of Li-species from $LiNbO_3$ substrates during growth of the films. The conducting layer intimately contacts the bottom electrodes (Cu-foil) by without forming the Schottky barrier, form homojunction with the insulating layer that facilitates injection of electrons into conduction band of diamond, and readily field emitted at low applied field. The EFE of freestanding UNCD films could be turned on at a low field of $E_0 = 10.0$ V/μm, attaining EFE current density of 0.2 mA/cm^2 at an applied field of 18.0 V/μm, which is superior to the EFE properties of UNCD films grown on Si substrates with the same chemical vapor deposition (CVD) process. Such an observation reveals the importance in the formation of homojunction on enhancing the EFE properties of materials. The large grain granular structure of the freestanding UNCD films is more robust against harsh environment and shows high potential toward diamond based electronic applications.

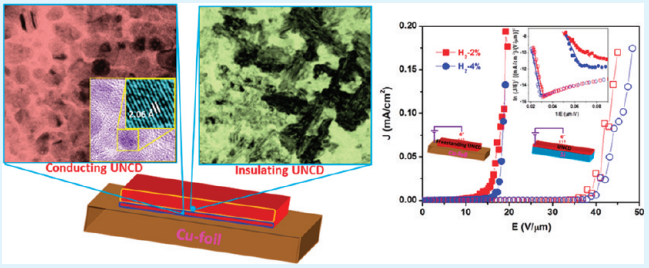

KEYWORDS: ultrananocrystalline diamond, freestanding films, homojunction interface, n-type semiconducting diamond, insulating diamond, electron field emission

1. INTRODUCTION

Electron field emitting micro/nanostructures of diverse materials, mainly semiconductor nanowires or nanotubes, carbon nanotubes, and diamond thin films, have been extensively investigated for their potential as cold cathode emitters.[1−6] The electron field emission (EFE) from cold cathode electron emitters is usually obtained by applying an electric field that causes electrons to tunnel from the materials surface into vacuum. However, practical application of the presently available cold cathode materials is limited because of their lack of reproducibility and irregularity.[5,6] In fact, films with flat surfaces and high EFE properties have great potential over the presently used complex field emitting structures that can considerably reduce the device fabrication cost. Among the field emitting materials, diamond is known for its negative electron affinity (NEA) surface and is a fascinating electronic material because of its unique physical or chemical properties and high thermal conductivity that can fuel devices with higher efficiencies.[6−11] Nevertheless, for the insulating diamond to be used as a cold cathode by effectively supplying electrons to its emitting surface is still a challenge. The typical problem can be the energy barrier between substrate and insulating diamond film, which may hinder the efficient supply of electrons to the top surface emission sites. Reports have been shown the enhanced EFE mechanism of diamond based on metal-diamond-vacuum triple junctions.[6,12,13] Though this emission mechanism has been found helpful, the interface issues and existence of electron transport barriers between the metal and diamond need to be considered, which may hinder the realization of a highly efficient electron emitter. It is clear that if electrons can efficiently supply to top emitting sites of insulating diamond, it can be readily field emitted due to NEA of the diamond surface,[6−11] and then the diamond will be the possible cold cathode material to replace the presently used materials.

On the other hand, ultrananocrystalline diamond (UNCD) films have been reported to show superior EFE behavior as compared to micrometer- or nanosized diamond films.[5,13,14] It is also known that n-type doping would be ideal to enhance the EFE properties of diamond. The possibilities to dope UNCD as n-type conducting by N, Li, or P doping and thereby forming a high field emitting diamond material owing an era toward diamond-based cold cathode applications.[15−24] Although the efforts to fabricate n-type conducting micrometer size diamond films by nitrogen doping were not beneficial as it was forming a

Received: July 2, 2011
Accepted: September 26, 2011
Published: September 26, 2011

dx.doi.org/10.1021/am200867c | *ACS Appl. Mater. Interfaces* 2011, 3, 4007–4013

deep donor level located about 1.7 eV below the conduction band (CB) minimum, the nitrogen doping into UNCD films is reported to show the n-type conductivity[16,17] as well as enhanced the EFE properties.[18−20] However, there exists some controversy, such as whether it is due to nitrogen doping effect or the induction of lattice defect that enhanced the EFE properties of UNCD films. Additionally, the N-doping temperature to create n-type conductivity for UNCD films was very high (about 800 °C),[16,19] therefore, we have recently adopted the Li-doping process that used $LiNbO_3$ substrate as the doping source and thereby fabricated n-type conducting UNCD films at low growth temperature (below 600 °C).[23]

Here we report the fabrication of novel electron field emitters made of freestanding insulating UNCD films with n-type conducting bottom layer, which could be attached to a metal contact. These novel structures could overcome the usually observed Schottky barrier for the electron transfer from metal to insulating diamond or semiconductor to diamond, by using an n-type conducting (semimetallic type) UNCD back layer to contact with metal back support. The insulating UNCD is grown in situ over the n-type layer and thereby the interface issues are limited. Thus, an efficient flat UNCD based field emitters are fabricated with overwhelming EFE properties as compared to UNCD films grown on n-type Si substrates under the same growth conditions. The detail structural properties of freestanding UNCD field emitters and possible mechanism of its high EFE characteristics are discussed.

2. EXPERIMENTAL METHODS

Freestanding UNCD films were fabricated using $LiNbO_3$ as substrates in a microwave plasma enhanced chemical vapor deposition system with 1200 W and 110 Torr for 4−10 h. Prior to the growth of the films, $LiNbO_3$ substrates were preseeded in a solution containing nanodiamond (about 4 nm in size) and titanium (365 mesh) powders in methanol for 45 min. Different amount of H_2 (2 or 4%) was added into CH_4(1%)/Ar plasma. The substrate temperature due to plasma bombardment effect (no external heater was used in the experiments) was measured with a thermocouple attached to the substrate holder and was estimated to around 510 and 540 °C for 2% and 4% H_2−CH_4/Ar plasma, respectively. The UNCD growth rate is about 400 nm/h and 600 nm/h for 2% and 4% H_2−CH_4/Ar plasma, respectively, which were estimated from cross-sectional field-emission scanning electron microscopic (FESEM, JEOL 6200) images (figures not shown). The freestanding films with the dimension of substrates were robotically detached from the substrates because of the difference in thermal expansion coefficient between diamond and $LiNbO_3$ substrate. The freestanding UNCD films were easily bonded on Cu-foil for characterizing their EFE properties. Figure 1 shows schematics of the processes for detaching UNCD films from $LiNbO_3$ substrates and the bonding of films to Cu-foil substrates. Another set of UNCD films were grown on n-type Si substrates under the same deposition conditions to facilitate comparison on their characteristics. Such kinds of films, designated as UNCD/Si films, were also directly bonded to Cu-foil by without detaching UNCD films from Si substrates for EFE characterization.

The morphologies and microstructures of the films were examined using FESEM and transmission electron microscopy (TEM; Joel 2100; operated under 200 eV), respectively. The Raman spectroscopic measurement (Renishaw, λ = 328 nm) was performed at room temperature. Hall measurements (ECOPIA) were carried out in a van der Pauw configuration to confirm *n*-type conductivity of the films. Prior to the Hall measurements, secondary ion mass spectroscopy (SIMS, Cameca-I4f) depth profile for the conducting side of the film was measured (figure not shown), which showed a typical depth of Li is diffusion into UNCD to be about 255 nm. EFE characteristics of the samples were measured using a molybdenum rod with diameter of 2 mm as anode and *I*−*V* characteristics were acquired using Keithley 237 electrometer. An applied field at a current density of 1 μA/cm^2 is taken as the turn-on field. The EFE behavior of materials is explained using Fowler-Nordheim (FN) theory.[25]

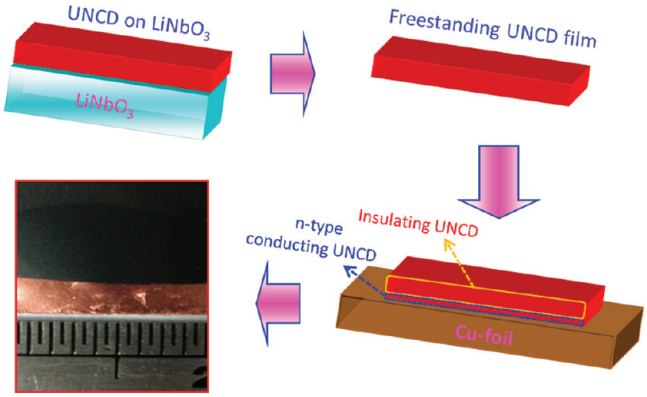

Figure 1. Schematic representations of fabrication and bonding processes of freestanding UNCD films and typical photograph of the film bonded to Cu-foil substrate.

3. RESULTS AND DISCUSSION

The UNCD films grown on Si-substrates (UNCD/Si) are highly insulating. The conductivity of the films was not measurable by van der Pauw Hall measurement method. Interestingly, the freestanding UNCD films show different properties for the two surfaces. While the top surface of freestanding UNCD films shows the same high insulting characteristics as the UNCD/Si films, the bottom surface, which was in contact with $LiNbO_3$ substrates during growth, are highly n-type conducting (Table 1). Measurements reveal that conducting side of the freestanding UNCD film grown in 2% H_2−CH_4/Ar plasma possesses a good conductivity of $\sigma = 5.6 \times 10^{-3}$ $(\Omega\ \mathrm{cm})^{-1}$ with sheet carrier density of $n = 1.4 \times 10^{12}$ cm^{-2} ($\sigma = 7.4 \times 10^{-3}$ $(\Omega\ \mathrm{cm})^{-1}$ and n=3.6 $\times$ 10^{13} cm^{-2} for 4% H_2−CH_4/Ar plasma grown freestanding film). Such a result infers that the freestanding UNCD films are of homojunction with top insulating and bottom conducting surfaces. The significance of such a homojunction characteristic on the EFE behavior of freestanding UNCD films will be discussed shortly.

UNCD films grown on Si and $LiNbO_3$ substrates possess similar surface morphology and crystallinity. Figure 2a indicates that these films contain elongated grains of about 20 nm × 400 nm in size, which is completely different from the equi-axed granular structure for the conventional UNCD films grown in 0% H_2−CH_4/Ar plasma (not shown). Moreover, Figure 2b shows that the Raman spectra for these films contain broaden Raman peaks, which are characteristics of diamond materials with ultrasmall grain granular structure. There are ν_1-band at 1185 cm^{-1}, representing the existence of transpolyacetylene phase at grain boundaries[26] and D*-band at 1365 cm^{-1} and G-band near 1575 cm^{-1}, representing the presence of disordered carbons or nanographites. Moreover, there appears a sharp resonance peak near 1332 cm^{-1} (D-band), which represents sp^3-bonds. The appearance of D-band resonance peak indicates the existence of large diamond grains in the films.

Table 1. Electrical Properties and Turn-on Field of Electron Field Emission for Insulating Surfaces of Freestanding UNCD Films and UNCD Films Grown on Si Substrates with Different H_2 % in CH_4(1%)/Ar Plasma

materials	H_2 % in CH_4 (1%)/Ar plasma (%)	sheet carrier[a,b] concentration (cm^{-2})	conductivity[a,b] ($1/\Omega$ cm)	turn-on field (V/μm)
freestanding	2	1.4×10^{12}	5.6×10^{-3}	10
UNCD	4	3.6×10^{13}	7.4×10^{-3}	12
UNCD/Si	2			33
	4			35

[a,b] The sheet carrier concentration and conductivity, which were deduced from the Hall measurements in van der Pauw configuration, are the characteristics of the conducting side of the freestanding UNCD films. The insulating side and the UNCD/Si films show very low conductivity.

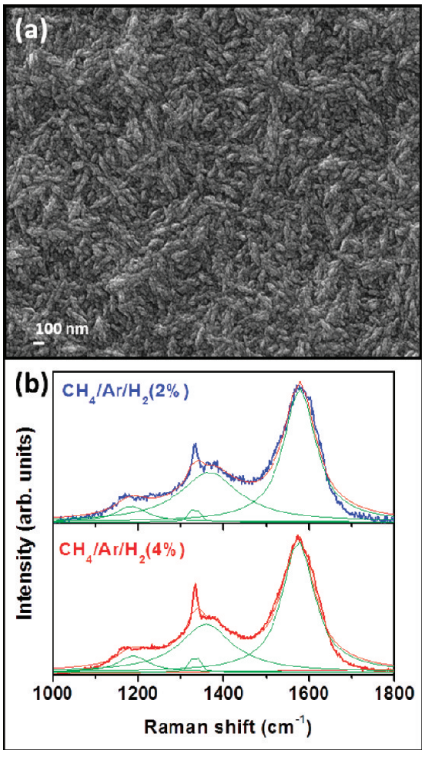

Figure 2. (a) Typical FESEM image and (b) UV Raman spectra of the insulating top surface of freestanding UNCD films grown with different H_2 % in the CH_4/Ar plasma.

Low-magnification TEM image for the insulating surface of freestanding UNCD film grown in 2% H_2-CH_4/Ar plasma is shown in Figure 3a, suggesting the formation of clusters of nanocrystalline diamond grains. It should be mentioned that, to prepare TEM foils, the samples were ion-milled from the interfacial side that was in contact with $LiNbO_3$ substrates, which means that the thin foil actually represents the region near top surface of the freestanding UNCD films. Higher magnification TEM image (Figure 3b) of marked area from Figure 3a clearly show dendrite type grains, which is also clearly visible from its merged dark field (DF) images taken from three different diffraction spots (shown in Figure 3c; red, green, and blue color circles) with the typical clusters of dendrite type grains orientation or formation due to the addition of H_2 in CH_4/Ar plasma. Further investigations using high magnification image of dendrite type grains (Figure 3d) and equivalent merged DF images (Figure 3e, f) corresponds to different diffraction spots shown in selective area diffraction (SAD) patterns (insets) also show the contribution from different clusters of grains with size of about 50−100 nm. HRTEM image in Figure 4 shows a complicated microstructure for the diamond grains as well as existence of stacking faults and corresponding Fourier-transform (FT) image (inset, FT) shows typical patterns for cubic diamond. Further investigation using FT images of selected areas marked as A−E suggest hexagonal structures of diamond grains, which are polymorphs (*nH*) of polycrystalline diamond.[27]

The microstructures of freestanding UNCD film grown in 4% H_2-CH_4/Ar plasma is similar with those shown in Figures 3 and 4, except that the size of large grains are slightly bigger (not shown). The UNCD/Si films grown with same CVD parameters also possess similar microstructure. It should be noted that such a microstructure (films grown in H_2-containing CH_4/Ar plasma) is totally different the conventional UNCD/Si films grown in 0% H_2-CH_4/Ar plasma. The conventional UNCD/Si films always have equi-axed granular structure with uniform small grains (~5 nm) and grain boundaries of considerable thickness (0.1−0.5 nm) containing disordered carbons.[27] The observed large-gain granular structure is in accord with the presence of sharp D-band resonance peak in the Raman spectra (cf. Figure 2b).

Figure 5 (open symbols) shows that the UNCD/Si films grown in 2% (or 4%) H_2-CH_4/Ar plasma require markedly larger field to turn on the EFE process ($(E_0)_{2\%H_2}$ = 33−35 V/μm) as compared with the EFE properties of the conventional UNCD/Si films that were grown in 0% H_2-CH_4/Ar plasma ($(E_0)_{0\%H_2}$ = 12.0 V/μm).[20] The higher turn-on field for UNCD/Si films is comparable with the EFE behavior of the typical good quality, large grain diamond films[28,29] and can be associated with the highly insulating characteristics of the films, which in turn is ascribed to the elimination of grain boundary phases due to the growth of large grains. There is no conduction path for transporting electrons to surface of the films. It is intriguing to observe that although the freestanding UNCD films possesses similar SEM morphology, Raman structure, and TEM microstructure with those of UNCD/Si films, these freestanding UNCD films exhibit markedly superior EFE properties to the UNCD/Si films. The EFE process for freestanding UNCD films could be turned on at 10−12 V/μm, attaining a large EFE current density of J_e = 0.20 mA/cm^2 at an applied field of 20.0 V/μm. The UNCD/Si films are essentially nonemitting at such a low applied field. The EFE parameters of these films are summarized in Table 1, along with the intrinsic electrical conductivity of the films.

Apparently, the superior EFE properties of the freestanding UNCD films, as compared to UNCD/Si films, are closely related to the phenomenon that the freestanding films possess a microstructure with homojunction interface characteristic. It has been observed that, in diamond like carbon (DLC) films, there always exist a large Schottky barrier at DLC-to-Si interface, which hinders markedly the transport of electrons from Si to DLC films and results in poor EFE properties for untreated DLC films.[30,31] For UNCD/Si films, there always forms an amorphous carbon layer near UNCD-to-Si interface. Large Schottky barrier at UNCD-to-Si interface, in addition to the insulating nature of UNCD diamond film, degrades the EFE properties of the films. In contrast, for the freestanding UNCD films, the surface in contact with the bottom electrode (the Cu-foil) is the highly conducting UNCD layer,

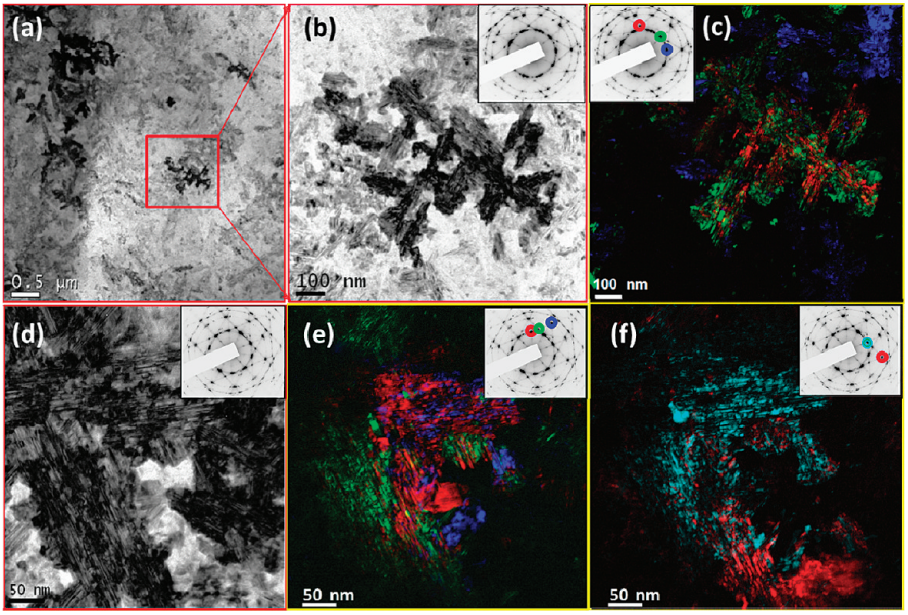

Figure 3. (a) Low-magnification TEM image of insulating surface of UNCD film, (b) higher-magnification image of the marked area shown in (a) and inset shows corresponding SAD pattern, (c) merged dark-field (DF) images of three different SAD spots (corresponds to b) marked with circles in different colors (red, green, and blue) as shown in the insets, and (d) high-resolution TEM (HRTEM) image of insulating side of UNCD and inset shows corresponding SAD pattern. (e, f) Merged DF images (corresponds to d) corresponding to the different SAD spots marked as circles in different colors as shown in the insets.

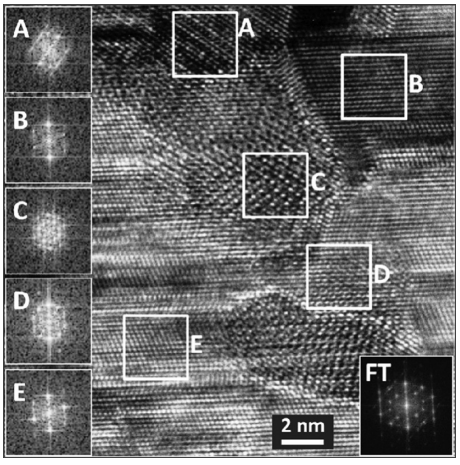

Figure 4. HRTEM image of typical insulating surface of UNCD film and inset shows its FT image. FT images of selected square areas marked as A−E are shown at the left side of the image.

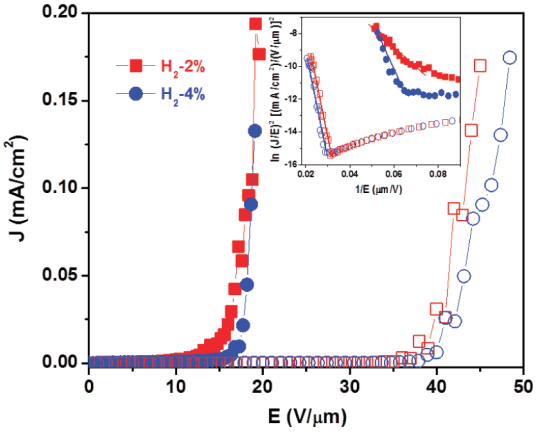

Figure 5. Comparison between the EFE properties of insulating surfaces of freestanding UNCD films (solid symbols) and UNCD films grown on Si substrates (open symbols) with different H_2 % in the CH_4/Ar plasma and inset is FN plot of the corresponding data.

which eliminates the formation of the Schottky barrier. Moreover, it is possible that the homojunction nature of freestanding UNCD films promoting transport of electrons from the conducting side to the insulating side of UNCD films. The electrons are transported from the bottom electrodes to all the way to the diamond surface without any barrier. Abundant supply of electrons, in conjunction with high mobility and NEA characteristics of diamond materials, renders the freestanding UNCD films as good EFE emitters.

The question remaining now is how the highly conducting UNCD materials formed when the films were grown on $LiNbO_3$ substrates. To investigate the possible formation mechanism, the microstructure of conducting side of freestanding UNCD films was examined using TEM. It should be noted that for the purpose of studying the microstructure of conducting side of freestanding UNCD films, the samples were ion-milled from the top surface of the films such that the thin foil mainly contains the materials near to the UNCD-to-$LiNbO_3$ interface.

Figure 6a shows typical HRTEM image of conducting side of the freestanding UNCD films. Surprisingly, these regions contain abundant nanosized clusters with 5−20 nm in size. The SAD pattern in inset of Figure 6b shows (111), (220) and (311) diffraction rings, which ensure that the clusters are UNCD grains (c-diamond; $Fd3m$).[27,32] The (200) forbidden reflection ring corresponds to n-diamond grains ($Fm3m$).[33,34] That is, the nanosized clusters are mainly diamond grains, which are randomly oriented. Investigations

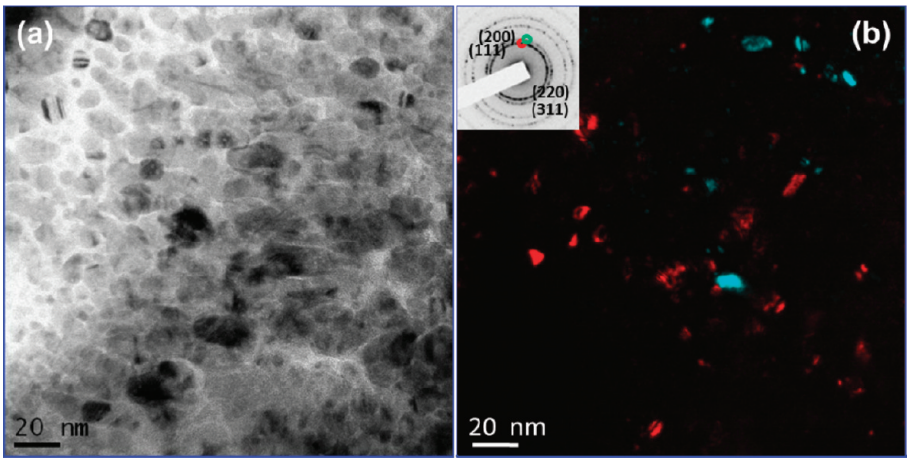

Figure 6. (a) High-magnification TEM image of conducting Li-doped surface of UNCD film and (b) equivalent merged DF images of two different SAD spots from (111) and (200) patterns marked with circles in red and light blue colors, respectively, shown in the inset contributing for c- and n-diamond grains.

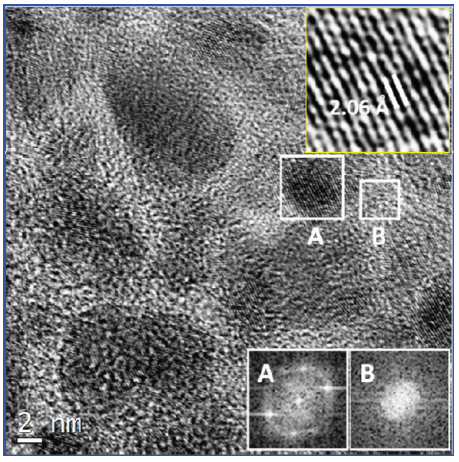

Figure 7. Typical HRTEM image of conducting Li-doped surface of freestanding UNCD film. The lattice image of UNCD grain (area A) and FT images of selected square areas marked as A and B are shown as insets.

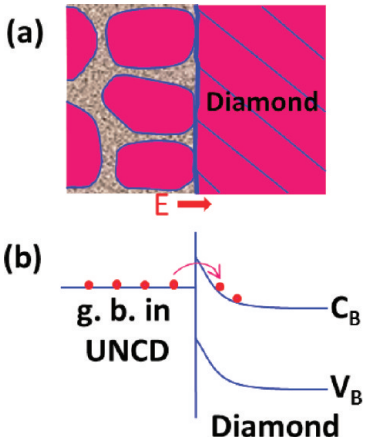

Figure 8. (a) Schematic representation of typical conducting-to-insulating transition layer (C-to-I region) of the freestanding UNCD films and (b) schematic band diagram corresponding to these regions.

using merged dark field (DF) images show different grains contributing for two selected diffraction spots from (111) and (200) rings (shown with red and light blue color circles) contributing for c- and n-diamond grains, respectively, which indicate the coexistence of 5−10 nm size c- and n-diamond grains in the conducting side of UNCD film (Figure 6a). HRTEM image in Figure 7 again confirm UNCD grain size of about 5−10 nm. The lattice image in the inset shows typical d-space of 0.206 nm for diamond grains. Formation of about 0.5−1 nm wide grain boundary nanochannel is also observed. The FT images show clearly the presence of c-diamond grains (area A, FT_A) and grain boundaries are mostly occupied with mixture of sp^2 or amorphous type carbon phases (area B, FT_B).

It is apparent that the doping of Li into UNCD could provide n-type conductivity and the dopant activation (or growth) temperature (<510 °C) is very low as compared to the required temperature for N doping (≥800 °C)[16,19] to observe the n-type conductivity. We have also found that substrate temperature is initially increases with growth time and saturates after 30 min and increasing amount of H_2 in the plasma also augments substrate temperature (figure not shown). The increase in substrate temperature must be contributing for higher amount of Li-diffusion into the films; however, that also enhances the faster dendrite type grain growth and insulating layer formation. How the Li-doping enhances the conductivity of UNCD films is not completely understood yet. It is possibly via a mechanism similar to that of N-doping on improving the conductivity of UNCD films, viz. the doped Li promotes the formation of disordered carbon containing nanochannels and resides at grain boundaries that provide grain boundary transport, i.e., electron injection into interband defect levels or to π^* states, and enhances the electron transport along grain boundaries.[17] Restated, it is possible that the doped Li resides in the grain boundary nanochannel and promotes the n-type conductivity, which is a similar mechanism as reported for N-doped UNCD films.

The other question, which is yet unsolved, is how the electrons transport from conducting region to insulating region of the freestanding UNCD films by without suffering the large interfacial potential barrier? Figure 8a schematically illustrates a typical conducting-to-insulating transition layer (C-to-I region) of the freestanding UNCD films. The conducting layer consists of insulating nanosized diamond clusters, which are separated by

a thin and conducting grain boundary phase (cf. Figure 6b).[16] In contrast, the insulating layer contains large insulating diamond grains, which are in contact with one another, i.e., the grain boundaries are thin and insulating (cf. Figure 3b). The electrons are mainly transport along the nanosized channels of the grain boundaries of the conduction regions toward the large diamond grains in insulating regions. The grain boundaries are presumed to contain hydrocarbon, such as conductive transpolyacetylene.[13,16,26] The electrons in the grain boundaries of the conduction regions experience large field enhancement factor because of the smallness in dimension of the filament-like geometry of the grain boundaries. Therefore, the electrons can tunnel through the interface at the "tip" of grain boundary filaments to CB of large diamond grains easily under the application of moderate external field. Some of the electrons may also tunnel to the ultrasmall diamond grains in the conduction layer during the transportation process, which further facilitates the transportation of electrons to the large diamond grains through the C-to-I interface. The electronic band diagram corresponding to such a microstructure is schematically illustrated in Figure 8b.

The phenomenon that the EFE behavior of an insulating diamond can be improved via the enhancement on the ejection efficiency for electrons from the back contact materials to the diamond, which, in turn, was achieved by increasing the roughness of the back contact surface has also been reported by Geis et al.[28] Similarly, the observed high EFE characteristics for the freestanding UNCD films, as compared with those of the UNCD/Si films, can be accounted for the fact that the electrons are transported from back electrodes to the conducting surface of freestanding UNCD films and then directly injected in to the CB of the insulating UNCD layer via quantum tunneling process. The injected electrons were transported through the diamond to the emitting surface and then emitted to vacuum without any difficulty because of the NEA nature of the diamond surface.[6,13,35,36] Restated, the tunneling of electrons is facilitated because of the formation of the homojuction interface between conducting and insulating UNCD layers. The EFE from insulating UNCD/Si is less efficient in the injection of electrons from Si substrate to CB of UNCD film and thus showed poor EFE characteristics as compared to the freestanding UNCD films.

The presence of graphite phase along the boundaries between diamond particles has been observed to markedly enhance the EFE properties of diamond/graphite composite materials.[35,37] Such observations are in accord with the conduction model proposed in Figure 8, viz. the existence of nanosized grain boundary phase in the conduction layer of freestanding UNCD films, which is the authentic factor for the enhanced EFE properties for the films. The other silent feature of these freestanding UNCD films is that the surface of the films actually contains diamond with large-grain granular structure. Such a large-grain diamond is chemically stable and is robust against the harsh environment. The surface of such a large-grain granular structure can be easily cleaned by plasma treatment process, without damaging the underlying conducting UNCD layers. The high EFE characteristics can be easily resumed. Such a characteristic is overwhelmingly advantageous over the conventional high EFE materials, such as carbon nanotubes, or nanoflakes, which is susceptible to degradation when exposed to harsh environment. No plasma treatment process can be applied for cleaning the surface of these nanocarbon materials by without inducing serious damage to the emitting materials.

4. CONCLUSIONS

In summary, a possible way is demonstrated to fabricate unique high field emitting freestanding insulating UNCD emitters with homojuction n-type conducting back layer. The freestanding films showed outstanding EFE properties as compared to UNCD/Si. Low temperature Li-diffusion into the films is presumed to promote the n-type conductivity, the formation of disordered carbon nanochannels, and grain boundary incorporation of Li. The formation of homojuction interface between conducting and insulating UNCD layers facilitated the tunneling of electrons, the injection of CB electrons form conducting side to the insulating UNCD layer, and their direct transport to emitting sites that are possibly the major reasons for high EFE properties for the freestanding films. The bonding of these novel freestanding UNCD films to desired substrates could make these films for device applications and may open up a pathway to their use in diamond electronics.

AUTHOR INFORMATION

Corresponding Author

*E-mail: peetijoseph@gmail.com (J.P.T); inanlin@mail.tku.edu.tw (I.N.L).

ACKNOWLEDGMENT

The authors thank the National Science Council, Republic of China for the support of this research through the project NSC99-2119-M-032-003-MY2.

REFERENCES

(1) Sun, M.; Gao, Y.; Zhi, C.; Bando, Y.; Golberg, D. *Nanotechnology* **2011**, *22*, 145705.

(2) Zhai, T.; Fang, X.; Bando, Y.; Dierre, B.; Liu, B.; Zeng, H.; Xu, X.; Huang, Y.; Yuan, X.; Sekiguchi, T.; Golberg, D. *Adv. Funct. Mater.* **2009**, *19*, 2423.

(3) Fan, S.; Chapline, M. G.; Franklin, N. R.; Tombler, T. W.; Cassell, A. M.; Dai, H. *Science* **1999**, *283*, 512.

(4) Shang, N.; Papakonstantinou, P.; Wang, P.; Zakharov, A.; Palnitkar, U.; Lin, I. N.; Chu, M.; Stamboulis, A. *ACS Nano* **2009**, *3*, 1032.

(5) Zhu, W.; Kochanski, G. P.; Jin, S. *Science* **1998**, *282*, 1471.

(6) Geis, M. W.; Efremow, N. N.; Krohn, K. E.; Twichell, J. C.; Lyszczarz, T. M.; Kalish, R.; Greer, J. A.; Tabat, M. D. *Nature* **1998**, *393*, 431.

(7) Yamaguchi, H.; Masuzawa, T.; Nozue, S.; Kudo, Y.; Saito, I.; Koe, J.; Kudo, M.; Yamada, T.; Takakuwa, Y.; Okano, K. *Phys. Rev. B* **2009**, *80*, 165321.

(8) Geis, M. W.; Deneault, S.; Krohn, K. E.; Marchant, M.; Lyszczarz, T. M.; Cooke, D. L. *Appl. Phys. Lett.* **2005**, *87*, 192115.

(9) Okano, K.; Koizumi, S.; Silva, S. R. P.; Amaratunga, G. A. J. *Nature* **1996**, *381*, 140.

(10) Krueger, A. *Adv. Mater.* **2008**, *20*, 2445.

(11) Watanabe, H.; Nebel, C. E.; Shikata, S. *Science* **2009**, *324*, 1425.

(12) Furkert, S. A.; Wotherspoon, A.; Cherns, D.; Fox, N. A.; Fuge, G. M.; Heard, P. J.; Lansley, S. P. *Appl. Phys. Lett.* **2007**, *90*, 242109.

(13) Krauss, A. R.; Auciello, O.; Ding, M. Q.; Gruen, D. M.; Huang, Y.; Zhirnov, V. V.; Givargizov, E. I.; Breskin, A.; Chechen, R.; Shefer, E.; Konov, V.; Pimenov, S.; Karabutov, A.; Rakhimov, A.; Suetin, N. *J. Appl. Phys.* **2001**, *89*, 2958.

(14) Pradhan, D.; Lin, I. N. *ACS Appl. Mater. Interfaces* **2009**, *1*, 1444.

(15) Kajihara, S. A.; Antonelli, A.; Bernholc, J. *Phys. Rev. Lett.* **1991**, *66*, 2010.

(16) Bhattacharyya, S.; Auciello, O.; Birrell, J.; Carlisle, J. A.; Curtiss, L. A.; Goyette, A. N.; Gruen, D. M.; Krauss, A. R.; Schlueter, J.; Sumant, A.; Zapol, P. *Appl. Phys. Lett.* **2001**, *79*, 1441.

(17) Williams, O. A.; Curat, S.; Gerbi, J. E.; Gruen, D. M.; Jackman, R. B. *Appl. Phys. Lett.* **2004**, *85*, 1680.
(18) Ikeda, T.; Teii, K. *Appl. Phys. Lett.* **2009**, *94*, 143102.
(19) Chen, Y. C.; Tai, N. H.; Lin, I. N. *Diam. Relat. Mater.* **2008**, *17*, 457.
(20) Joseph, P. T.; Tai, N. H.; Lee, C. Y.; Niu, H.; Pong, W. F.; Lin, I. N. *J. Appl. Phys.* **2008**, *103*, 043720.
(21) Goss, J. P.; Briddon, P. R. *Phys. Rev. B* **2007**, *75*, 75202.
(22) Sternschulte, H.; Schreck, M.; Stritzker, B.; Bergmaier, A.; Dollinger, G. *Diam. Relat. Mater.* **2000**, *9*, 1046.
(23) Joseph, P. T.; Tai, N. H.; Lin, I. N. *Appl. Phys. Lett.* **2010**, *97*, 042107.
(24) Okumura, K.; Mort, J.; Machonkin, M. *Appl. Phys. Lett.* **1990**, *57*, 1907.
(25) Fowler, R. H.; Nordheim, L. *Proc. Royal Soc. Lond. A* **1928**, *119*, 173.
(26) Ferrari, A. C.; Robertson, J. *Phys. Rev. B* **2001**, *63*, 121405.
(27) Wang, C. S.; Chen, H. C.; Cheng, H. F.; Lin, I. N. *J. Appl. Phys.* **2010**, *107*, 034304.
(28) Geis, M. W.; Twichell, J. C.; Efremow, N. N.; Krohn, K.; Lyszczarz, T. M. *Appl. Phys. Lett.* **1996**, *68*, 2294.
(29) Bozeman, S. P.; Baumann, P. K.; Ward, B. L.; Powers, M. J.; Cuomo, J. J.; Nemanich, R. J.; Dreifus, D. L. *Diamond Relat. Mater.* **1996**, *5*, 802.
(30) Robertson, J.; Rutter, M. J. *Diamond Relat. Mater.* **1998**, *7*, 620.
(31) Robertson, J. *Thin Solid Films* **1997**, *296*, 61.
(32) Hsu, C. H.; Cloutier, S. G.; Palefsky, S.; Xu, J. *Nano Lett.* **2010**, *10*, 3272.
(33) Hirai, H.; Kondo, K. *Science* **1990**, *253*, 772.
(34) Prawer, S.; Peng, J. L.; Orwa, J. O.; McCallum, J. C.; Jamieson, D. N.; Bursill, L. A. *Phys. Rev. B* **2000**, *62*, 16360.
(35) Cui, J. B.; Stammler, M.; Ristein, J.; Ley, L. *J. Appl. Phys.* **2000**, *88*, 3667.
(36) Wisitsora-at, A.; Kang, W. P.; Davidson, J. L.; Kerns, D. V. *Appl. Phys. Lett.* **1997**, *71*, 3394.
(37) Karabutov, A. V.; Frolov, V. D.; Pimenov, S. M.; Konov, V. I. *Diamond Relat. Mater.* **1999**, *8*, 763.